The three-dimensional light field within sea ice ridges

Christian Katlein[1, 2], Jean-Philippe Langelier[3], Alexandre Oellet[3], Félix Lévesque-Desrosiers[3], Quentin Hisette[4], Benjamin A. Lange[5], Simon Lambert-Girard[2], Marcel Babin[2], Simon Thibault[3]

[1]Alfred-Wegener-Institut Helmholtz Zentrum für Polar- und Meeresforschung, Bremerhaven, Germany.

[2]Takuvik Joint International Laboratory, Université Laval and CNRS, Québec, Canada.

[3]Centre d'Optique, Photonique et Laser (COPL) and Département de Physique, de Génie Physique et d'Optique, Université Laval, Québec, Canada

[4]Hamburg Ship Model Basin (HSVA), Hamburg, Germany.

[5]Norwegian Polar Institute, Fram Centre. Tromsø, Norway

*Corresponding author: Christian Katlein (Christian.Katlein@awi.de)

Key Points:

- Computation of the full three-dimensional light field inside a pressure ridge
- Enhancement of scalar irradiance within the ridge
- Macro-pores act as light guides through the ridge

Abstract (150 words)

Sea ice pressure ridges have been recognized as important locations for both physical and biological processes. Their complex structure and internal geometry render them hard to study by field methods. To calculate the in- and under-ridge light field, we combined output from an ice mechanical model with a Monte-Carlo ray tracing simulation. This results in realistic light fields showing that light levels within the ridge itself are significantly higher than in the surrounding level ice. Light guided through ridge cavities and scattering in between ridge blocks also results in a more isotropic ridge-internal light field. While the true variability of light transmittance through a ridge can only be represented in ray tracing models, we show that simple parameterizations based on ice thickness and accounting for macro pores allow an estimation of mean light levels underneath ridges with reasonable accuracy.

Plain Language Summary

When two slabs of sea ice collide, they can break and form pressure ridges by piling up loose ice blocks over each other. The light environment within these ridges is very complicated, but also crucial for their characteristics as habitat for the sea ice ecosystem. We calculate the light field within and underneath such a pressure ridge by tracing the path of many individual photons through the ridge geometry. Our results show, that light levels within the ridge can be higher than in the adjacent undeformed ice. We suggest simple equations to estimate the light intensity underneath the pressure ridge, based on ice geometry data that can be obtained in the field.

1. Introduction

Investigating the optical properties of sea ice is an important key to accurately understand the energy transfer across the atmosphere-ice-ocean boundary. Recent changes in the physical properties of the Antarctic and, more notably the Arctic sea ice cover have resulted in increased light transmittance of the ice pack with important consequences for the physical and biological systems [*Meier et al.*, 2014; *Nicolaus et al.*, 2012]. A large number of studies have investigated the optical properties of sea ice, but most studies focused on undeformed, level and relatively more homogeneous sea ice. While some studies include deformation features such as pressure ridges [*Katlein et al.*, 2019; *Lange et al.*, 2017a; *Massicotte et al.*, 2019], there has been no dedicated investigation of the light field within and underneath these features.

Sea ice pressure ridges form during periods of ice convergence, when two slabs of sea ice collide, shear and break up into blocks that pile up above and below the water line [*Davis and Wadhams*, 1995; *Timco and Burden*, 1997]. The portion above the water line is called the ridge sail and is important for snow accumulation and atmospheric turbulence. The 4-5 times thicker portion underneath the water line is called the ridge keel [*Timco and Burden*, 1997], which determines the hydrodynamic interaction between ice and ocean [*Castellani et al.*, 2015; *Castellani et al.*, 2014], and provides shelter to ice associated flora and fauna [*Gradinger et al.*, 2010; *Hop et al.*, 2000; *Horner et al.*, 1992]. Newly formed ridges are a loose pile of individual ice blocks, characterized by significant macro-pore spaces in between the blocks [*Strub-Klein*

and Sudom, 2012]. This complex geometry of blocks and cavities in a newly formed ridge is very difficult to investigate, but it is exactly this complexity that gives rise to the unique and characteristic physical and biological processes associated with sea ice ridges. With time, thermodynamic processes cause the ridge to refreeze and consolidate in its inner part, while the edges of blocks melt into rounded shapes [*Høyland*, 2002]. Thus, older pressure ridges transform into more homogeneous, weathered and thick ice bodies – also known as hummocks – over several years [*Wadhams and Toberg*, 2012].

According to diving observations, the complex internal geometry of pressure ridges provides shelter for all trophic levels of the ice associated ecosystem forming a biological hotspot [*Assmy et al.*, 2013; *Hop et al.*, 2000; *Horner et al.*, 1992; *Melnikov*, 1997; *Melnikov and Bondarchuk*, 1987; *Siegel et al.*, 1990]. In addition to the ridges housing a particular microbial community [*Ackley*, 1986], small cavities provide physical protection from larger predators and ocean currents. Various algal communities thrive either hanging between ridge blocks [*Lange et al.*, 2017a; *Melnikov*, 1997] or growing on the upward facing block sides [*Fernández-Méndez et al.*, 2018]. On the leeward side of ridges, surface ice relative currents are much reduced increasing the ability of phytoplankton and zooplankton to avoid being flushed away [*Katlein et al.*, 2014]. Smaller cavities provide shelter for fish such as the polar cod, while the bigger macro-pores also provide a home and hunting ground for seals [*Furgal et al.*, 1996; *Smith et al.*, 1991]. Even polar bears are seeking shelter from the wind in between ridges and hunt for prey in ridge-associated seal lairs [*Pilfold et al.*, 2014]. Overall pressure ridges are the most prominent and ubiquitous structuring element of the sea ice landscape which despite their very dynamic evolution are home to a condensed and highly productive form of the sea ice associated ecosystem.

While sea ice thickness in the Arctic is declining [*Haas et al.*, 2008; *Kwok and Rothrock*, 2009] and the ice pack has gotten more dynamic [*Rampal et al.*, 2009], it is uncertain whether the role of sea ice ridges will become more or less important within the Arctic ecosystem. While the absolute size and frequency of multiyear ice ridges are likely to reduce [*Maslanik et al.*, 2007; *Maslanik et al.*, 2011], smaller and younger –and thus more porous– ridges are likely to make up the Arctic ice pack in the future [*Wadhams and Toberg*, 2012]. Investigations of physical properties, such as temperature, salinity and strength of pressure ridges, have been conducted intensively, as the mechanical properties are of commercial interest to shipping and

offshore operations [*Leppäranta and Hakala*, 1992; *Richter-Menge and Cox*, 1985; *Strub-Klein and Sudom*, 2012]. Underwater investigations of ridges have only recently been aided by robotic vehicles [*Fernández-Méndez et al.*, 2018; *Katlein et al.*, 2014; *Lange et al.*, 2017a].

Light is one of the main drivers particularly of the autotrophic portion of the ice associated ecosystem, and it is very important to understand the nature and amount of light present within the ecological hotspots of ridge cavities. However, radiative transfer in such complex geometries cannot be investigated with the typical one-dimensional radiative transfer models, as they are only formulated for homogeneous slabs of ice [*Katlein et al.*, 2016]. Thus, only few studies explicitly investigate the complex light field underneath ridges and hummocks [*Lange et al.*, 2019; *Lange et al.*, 2017b] or try to parameterize them for model calculations [*Fernández-Méndez et al.*, 2018; *Lange et al.*, 2017a]. To improve habitat characterization and the representation of pressure ridges in ecological models, it is necessary to improve our understanding of radiative transfer in complex ridge geometries.

The objective of our work is to explicitly model the light field geometry within and underneath a typical young pressure ridge. As field data of the full internal geometry of a pressure ridge are not yet available, we use an artificial ridge generated in an ice mechanical model as input for a three-dimensional ray-tracing radiative transfer model. Analysis of model output allows for the comparison of existing and new parameterizations of radiative transfer through sea ice pressure ridges.

2. Materials and Methods

2.1 Sea ice model and the investigated ridge

There are plenty of available datasets from surface laser scanning and underwater multibeam sonar surveys that can provide the full three-dimensional external geometry of pressure ridges [*Melling et al.*, 1993; *Williams et al.*, 2013; *Williams et al.*, 2015]. However, none of these studies provide insight into the internal structure of these complex ice geometries. Extensive drilling surveys [*Høyland*, 2002; *Strub-Klein and Sudom*, 2012] or geophysical methods, such as electromagnetic induction sounding [*Hunkeler et al.*, 2016] and nuclear magnetic resonance [*Nuber et al.*, 2017; *Rabenstein et al.*, 2013] can provide some information on the internal ridge structure. The spatial resolution and contrast of these data are, however, not sufficient as input data for precise three-dimensional radiative transfer modeling.

To overcome this lack of data, we use an artificially created ridge geometry from a mechanical sea ice model used for simulating the interaction of sea ice with ships and structures [*Hisette et al.*, 2017]. In this model, a ridge is created using the "floating-up" technique, where buoyant ice blocks are released underneath a level ice sheet of 1m thickness and afterwards formed into a ridge of triangular cross section. During the forming process, the ice blocks are pressed against each other so that a realistic ice-water porosity level is reached (An animation of this process can be found here: https://www.youtube.com/watch?v=Zwn2J39EOlA). This creation mechanism results in a ridge without sail (Figure 1a), but the continuous ice sheet comes closer to a partly consolidated ridge than a simulation where ridge blocks are piled up by moving two ice sheets against each other. The ridge construction method resulted in a macroporosity just above 25% in the ridge keel. Of course, this ridge can only approximate a realistic situation, as many real processes, such as consolidation and snow accumulation are not taken into account. The geometric size of the model domain (Figure 1b) is 74m by 63m with a maximum ridge keel depth of 6.64 m.

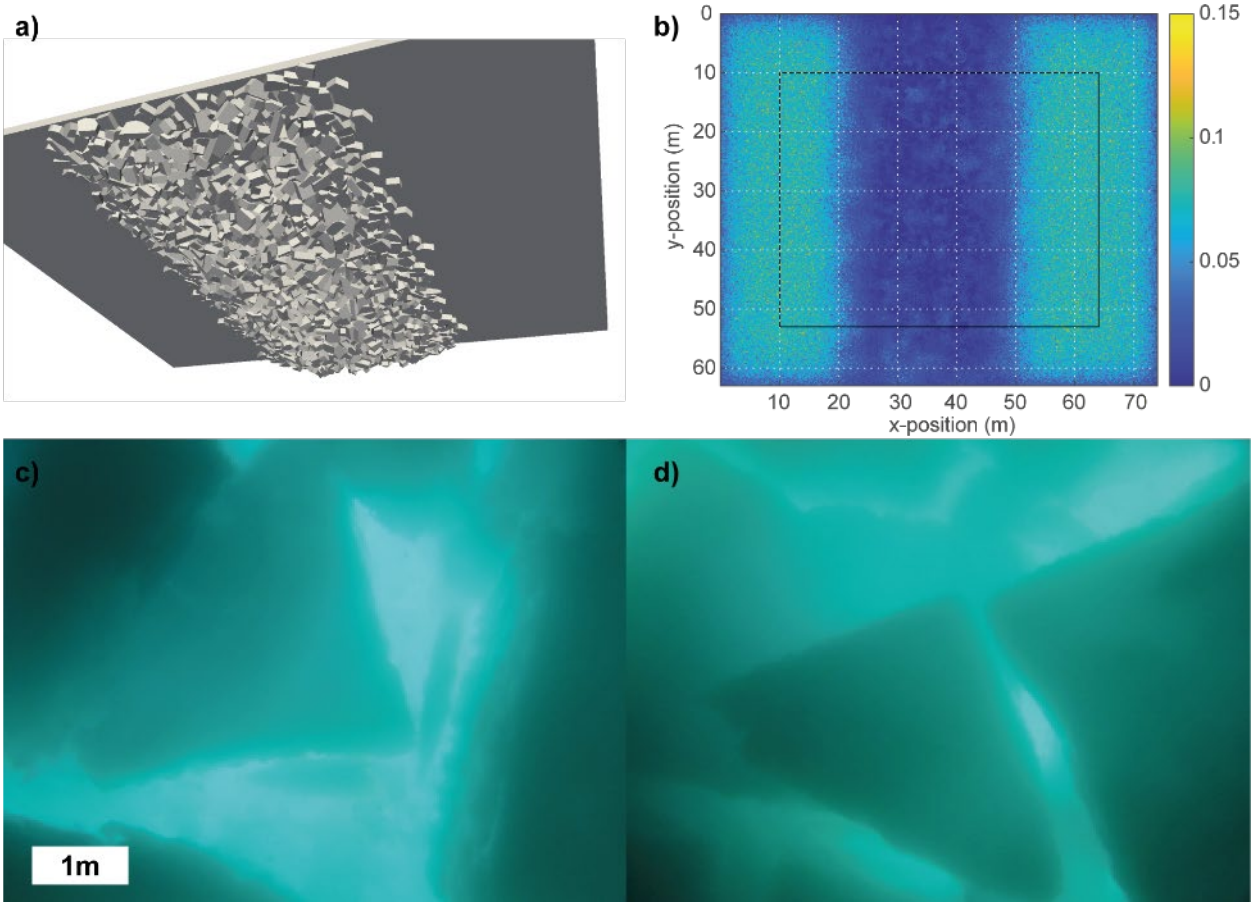

Figure 1. a) rendering of the investigated three-dimensional ridge geometry b) computed downward planar irradiance field at 4m depth. The black rectangle depicts the area used for data analysis. c&d) upward looking photos taken by a remotely operated vehicle from 19 August 2018 during the AO18 expedition with the Swedish icebreaker Oden from approximately 10m depth.

2.2 Optical Model

The three-dimensional ridge geometry from the mechanical ice model was directly used in the optical design software Zemax Optic-Studio (Zemax LLC, Kirkland, USA). Ray tracing was performed with a total number of $5 \cdot 10^7$ rays using a diffuse lambertian light source representative of typical cloudy conditions in the summer sea ice area. We assigned homogenous optical properties to the ice resulting in broadband transmittance of 7.4 % and albedo of 72 % for the 1m thick level ice sheet which is comparable to published literature values [*Katlein et al.*, 2019; *Katlein et al.*, 2021; *Light et al.*, 2008; *Light et al.*, 2015] . The Lambertian light source

emitted a realistic solar spectrum, and a database of measured real and imaginary refractive indices for ice was used [*Warren and Brandt*, 2008]. The water was assumed to be free of scatterers, representing clear Arctic waters. The scattering coefficient of the ice was set to $\kappa_{si} = 200\ m^{-1}$ and we adopted a Henyey-Greenstein phase function with asymmetry parameter $g = 0.94$. For the real and imaginary refractive index of water we used the database "Water" built into Optic-Studio stock materials catalog MISC. Total scalar (E_0) and downwelling planar irradiances (E_d) were calculated at a spatial resolution of 0.2 by 0.2 m by the model at horizontal levels of 0, 1, 2, 3, 4, 5 and 6 m depth, both within the ice and in the underlying water. Downwelling planar irradiance E_d quantifies the energy flux across a horizontal area, and thus includes a cosine weighting of rays depending on zenith angle. Total scalar irradiance E_0 quantifies the energy flux through a point integrating equally weighted rays from all directions. We define the ratio $m = E_d/E_0$, which is similar to the mean cosine $\mu = E_{net}/E_0$ [*Mobley*, 1994] and is a rough index describing the geometric shape of the angular radiance distribution.

To overcome edge effects of the discrete ray tracing simulation, only the central part of the simulated ridge was used in the following evaluation (Figure 1b). The resulting light fields closely resemble upward looking images obtained from under-ice ROV dives (Figure 1 c, d) showing that light field calculations of the ray tracing model generate realistic results.

2.3 Light field parameterizations

Most light transmittance parameterizations have been designed for level ice. Sea ice is often modeled as a plane parallel medium with homogenous material properties within one or several layers [*Mobley et al.*, 1998; *Perovich*, 1990]. Only simple parameterizations based on the exponential decay of light in a medium [*Bouguer*, 1729; *Lambert*, 1760] have been applied to the more complex situation for ice hummocks [*Lange et al.*, 2017a] and pressure ridges [*Fernández-Méndez et al.*, 2018].

The first parameterization that we evaluate in this study is the simple bulk-exponential approach. Light transmittance T is defined as the ratio of downwelling planar irradiance transmitted through the ice E_d divided by incoming downwelling planar irradiance at the ice surface E_i:

$$T = \frac{E_d}{E_i} \qquad (1)$$

Analogously scalar light transmittance is defined as the ratio of total scalar irradiance transmitted through the ice divided by incoming downwelling planar irradiance at the ice surface. In its most simple form of a uniform slab of ice light transmittance can be parameterized as [*Katlein et al.*, 2015; *Lange et al.*, 2017a]

$$T = (1 - \alpha) \cdot \exp(-\kappa_{d,ice} \cdot z), \qquad (2)$$

where α is the surface albedo and z the total bulk ice thickness. In our model setup of level ice without vertically varying optical properties, the optical properties described in section 2.2 yield a vertical attenuation coefficient for ice of $\kappa_{d,ice} = 1.33\ m^{-1}$.

For the more complex geometry of pressure ridges *Fernández-Méndez et al.* [2018] separated this formulation into a piecewise exponential plane parallel model, taking into account water pockets within the ice and several layers of ridge blocks. Adjusting their parameterization to our more idealized ridge results in

$$T = (1 - \alpha) \cdot \exp(-\kappa_{d,ice} \cdot (z_{ice,1} + z_{ice,2} + \cdots) - \kappa_{d,w} \cdot (z_{w,1} + z_{w,2} + \cdots)). \qquad (3)$$

Here $z_{ice,1} + z_{ice,2} + \cdots = \sum_{i=1}^{n} z_{ice,i}$ describes the sum of ice thickness associated with n individual ridge blocks and $z_{w,1} + z_{w,2} + \cdots$ the respective geometric thickness of water in the ridge voids. In the following the first is referred to as the partial ice thickness, which can also be imagined as the amount of ice that would need to be drilled during a vertical ridge drilling exercise. While this formulation seems to explicitly account for a more realistic ice geometry, it clearly neglects laterally traveling light. Total bulk ice thickness z (including voids) and partial ice thickness were extracted in all locations across the ridge. The average vertical attenuation coefficient in the water $\kappa_{d,w} = 0.02\ m^{-1}$ was determined from our simulation by fitting an exponential decay to the light field underneath level ice. The respective light transmittance was then calculated for each point using the above parameterization to allow for a comparison to the fully three-dimensional ray tracing model.

3. Results and Discussion

3.1 Calculated light field

The resulting calculated light fields are shown in Figure 2. Apart from the slow decay of light with depth under level ice due to water absorption, the model also reproduces the general

effect of lower light transmittance underneath the pressure ridge. Distinct shadows by individual ridge blocks are visible. These are also evident from upward looking ROV images (Figure 1c, d).

A main result from these calculations is that the scalar irradiance within the pressure ridge is considerably higher than at the same depth underneath level ice, particularly in the upper half of the ridge. This effect is caused by two factors. First, water filled cavities in the ridge lead to less total light attenuation. Second, the strong multiple scattering between ridge blocks changes the light field shape towards a more isotropic radiance distribution. This increases, particularly, the total scalar irradiance versus downwelling planar irradiance (Figure 2) as evident by the decreased mean cosine (section 3.2). Thus, light levels within ridge cavities are similarly high as within ridge blocks. These significantly higher light levels provide pelagic and ice associated algae and zooplankton with favorable light conditions within the ridge cavities. In their interior, ridges thus represent areas of higher light availability compared to the surroundings. In addition, macro pore space increases the habitable volume of the ridge offering also increased areas of ice surfaces as substrate. Only underneath, ridge keels shade the light field and decrease light transmittance. This particular light regime might further enhance positive factors such as the physical protection from currents and predators that the ridge associated ecosystem can benefit from [*Gradinger et al.*, 2010].

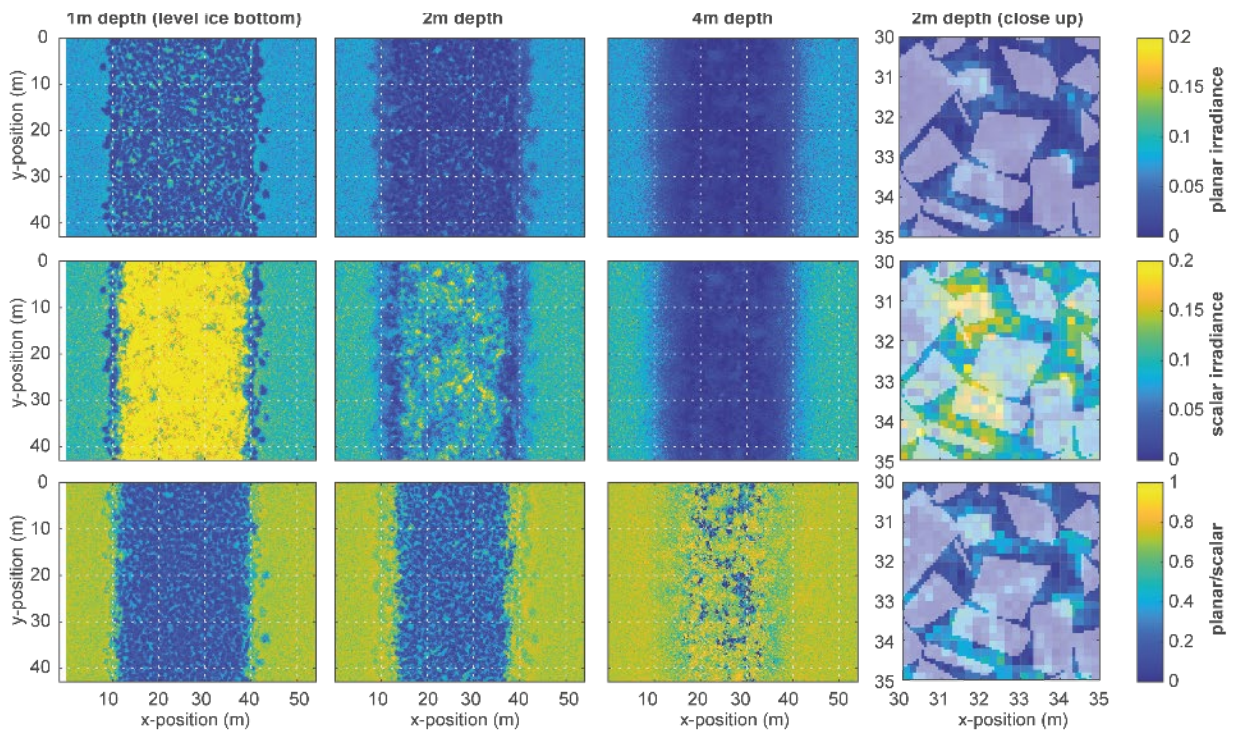

Figure 2: Horizontal slices of the calculated light field, within and underneath the ridge. Top row: planar downwelling irradiance (normalized to ice surface) at the depths of 1m, 2m, and 4m as well as a close up of the 2m depth within the ridge. Second row: Scalar irradiance. Third row: the ratio $m = E_d/E_0$ indicating the geometry of the light field.

3.2 Geometry of the light field in and underneath the ridge

Here, we use the ratio $\boldsymbol{m = E_d/E_0}$ as a descriptor of the light field geometry. It describes the radiance distribution geometry between the two extreme cases of isotropic ($\boldsymbol{m = 0.25}$) and unidirectional ($\boldsymbol{m = 1}$) light fields. Values of $\boldsymbol{\mu < 0.25}$ resemble a stronger upwelling portion of the light field caused by the upward-scattering of laterally travelling photons. Note, that this definition is different to the more common definition of the mean cosine of the downwelling light field as used in Matthes et al. [2019]. It is however equivalent in the absence of upwelling light, e.g. here under the level ice portion. As already mentioned above, multiple scattering within and in between ridge blocks bounces downwelling light back upwards within the ridge, while the low amount of scattering in the water column reduces upwelling light underneath ice. Organisms within the ridge thus receive similar amounts of light from all directions enhancing light availability for photosynthesis. Our model produces values of$\boldsymbol{m =}$

248 $\mathbf{0.72}$ comparable to the mean cosines shown by Matthes et al. [2019] for level ice (Figure 2). It
249 also reproduces the known slow increase of the mean cosine with depth. Within the ridge,
250 however, values are significantly lower. Values around $\boldsymbol{m = 0.1 - 0.3}$ indicate an isotropic or
251 directional in-ridge light field, where a majority of the light travels horizontally and not in
252 downwelling direction. Knowledge of these ratios enables easier parameterizations of scalar
253 irradiance levels within ridges.

254 **3.3 Comparison to simple ridge models**

255 Figure 3 evaluates the simple parameterizations of light transmission presented in section
256 2.3. Transmittance parameterized on the basis of total ice thickness is expectedly lower than
257 transmittance parameterized on the basis of partial ice thickness (Figure 3). Both
258 parameterizations do not appropriately account for lateral smoothing of light transmittance
259 pointing to the fact that estimations of the light field within a ridge from drill holes can both
260 over- and underestimate the actual light intensity. This is caused by the strong variability of
261 partial and total ice thickness along the ridge given by the chaotic block structure (Figure 4a).

262 Across ridge light profiles show a significant variability linked directly to local ridge
263 block geometries (Figure 4b). Deviations are most prominent when ridge cavities of large
264 vertical extent act as light guides through the ridge. While in our scenario we are able to evaluate
265 local partial and total ice thickness in each spot, this will not be possible in a real setting, where
266 ridge macroporosity data is acquired by ridge drilling. It is, however, evident that mean across-
267 ridge light transmittance between raytracing and exponential models fit reasonably well. The
268 parameterization using total ice thickness underestimates light transmittance, while the
269 parameterization using partial ice thickness comes much closer to the average. Thus,
270 parameterizations based on partial ice thickness will yield more realistic results. Both
271 parameterizations fail to reproduce the light field at the outer ridge slopes, which are
272 significantly smoother in the full three-dimensional simulation, than in the average
273 parameterizations due to horizontal light propagation (Figure 4).

274

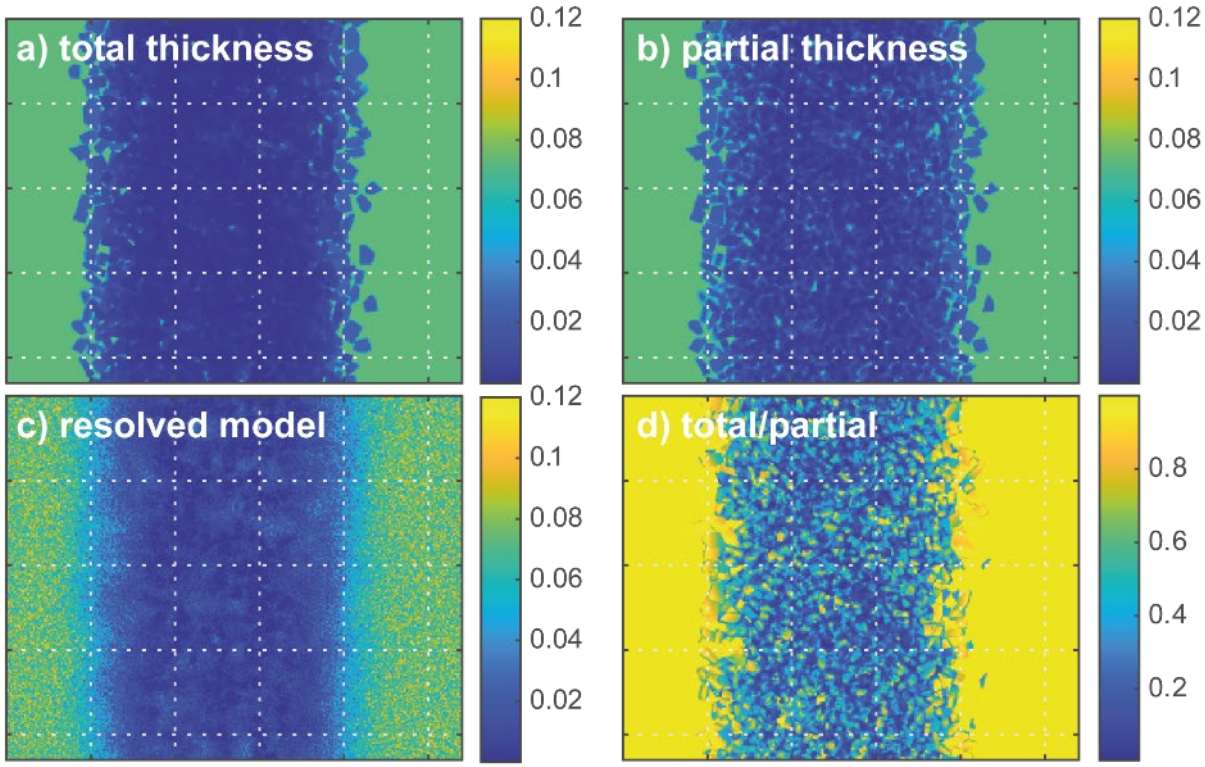

Figure 3: Light field at 5m depth as parameterized based on total ice thickness (a), partial ice thickness (b) and derived from the fully resolved three-dimensional model. Panel d) shows the ratio of the parameterizations based on total and partial sea ice thickness.

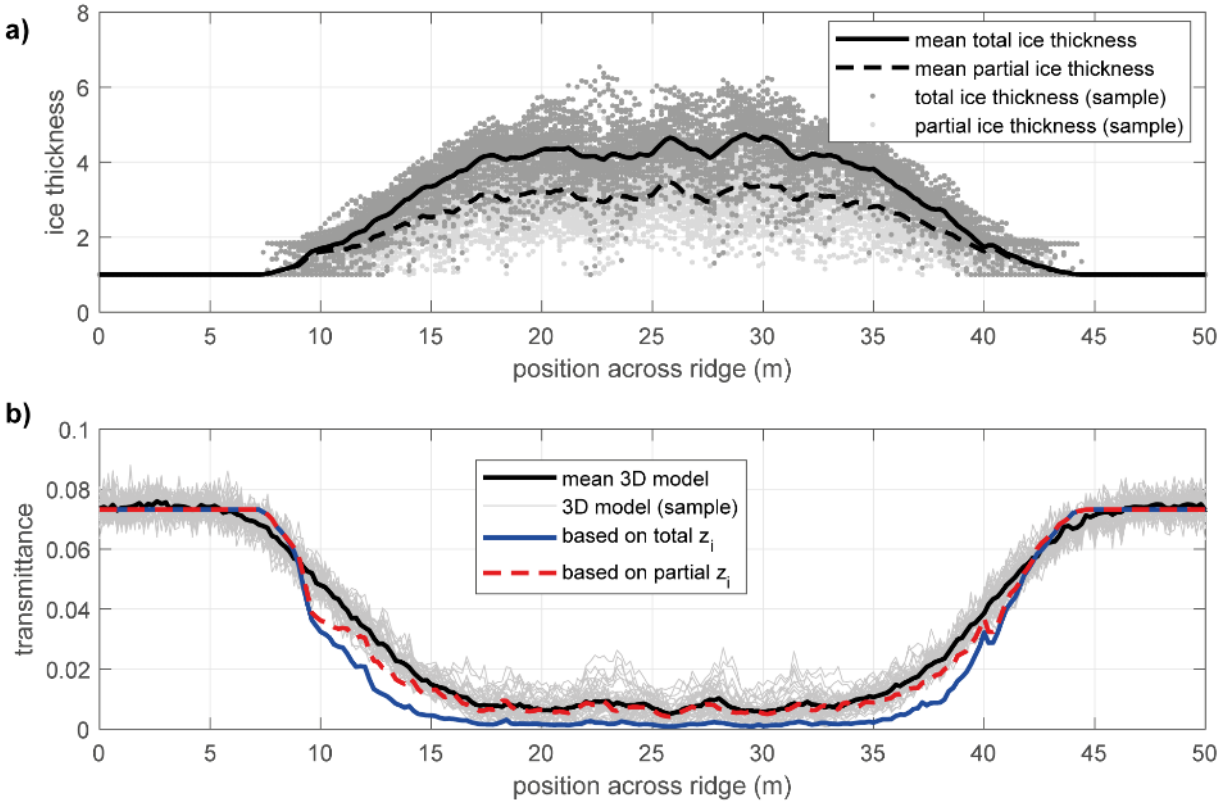

Figure 4: a) Across-ridge profiles of mean total (solid line) and partial (dashed line) ice thickness. Light and dark grey dots represent individual pixels of partial and total ice thickness respectively. b) Across ridge planar irradiance profiles: mean planar irradiance transmittance (solid black line) and individual profiles of planar irradiance transmittance at 5m depth from raytracing (thin grey lines), and parameterized using partial (dashed blue line) and total ice thicknesses (solid blue line).

3.4 Potential impact of the ridge sail

In our model setup, the introduction of a simple idealized ridge sail did not show any significant effect. However, in reality a ridge sail may have additional influences on the light field within and under the ridge keel by influencing the distribution of snow around the sail, and/or the additional geometric effects and scattering of light within the surface ice blocks and air gaps of the sail. Snow distribution is largely controlled by the surface topography of the sea ice where snow is removed from high points (e.g., ridge sails and hummocks) and accumulates in low points or adjacent to high points (e.g., around ridge sails) [*Lange et al.*, 2019; *Sturm et al.*, 2002]. This results in thick snow accumulation around ridges, typically greater than 0.5 m, substantially reducing the amount of light transmitted at those specific locations. The ridge sail, on the other hand, can have substantial regions of thin and snow-free ice, which may have an

298 important added influence on the light field by increasing light transmittance. Furthermore, the
299 geometry of the surface blocks (i.e., angle relative to the solar inclination) may provide a more
300 direct surface for solar radiation (i.e., decreasing the effective angle of inclination) minimizing
301 specular reflection and increasing light penetration into the ridge. These potential impacts and
302 uncertainties should be included and assessed in future modeling studies and field measurements
303 in order to quantify their respective effects.

304 **5. Summary**

305 We presented the first full three-dimensional modeling of the light field in a young
306 pressure ridge. Model results are comparable to observations from upward looking under-ice
307 cameras and thus are likely representative of a typical real-world situation. Light levels within
308 ridge cavities are up to three times higher than in the surrounding waters, thus enhancing the
309 ecological importance of pressure ridges for the sea ice system. The ridge light field is
310 characterized by an isotropic or even upwelling radiance distribution with low values of the
311 mean cosine. The high spatial variability of ridge block geometry can only be addressed
312 correctly in a full ray tracing calculation, but simple parameterizations provide a reasonable
313 mean estimate of both light transmittance and spatial variability. Parameterizations based on
314 partial ice thickness yield more realistic results by accounting for macroporosity of the ridge
315 structure. It is also evident that such simple parameterizations cannot correctly reproduce the
316 light field at the edge of ridges due to the importance of lateral light propagation.

317 Further and more complex assessment of realistic scenarios requires precise knowledge
318 of the full internal structure of pressure ridges, which is hard to acquire from field data. This also
319 applies to the complex interplay of ridge sails and snow accumulation and their effect on the
320 light field under water and within the ridge. As such field data will likely not become available
321 soon, simple parameterizations considering average ridge macro-porosity will allow for
322 reasonable estimates of the light field around pressure ridges.

323 **Acknowledgments**

324 The writing of this manuscript was supported by a postdoctoral research fellowship to CK by
325 Sentinel North supervised by Marcel Babin and Simon Thibault. The ROV work was funded by
326 the Helmholtz Infrastructure Initiative “Frontiers in Arctic Marine Monitoring (FRAM)” and the
327 Alfred-Wegener Institute. ROV observations during the AO18 expedition were supported by

captain and crew of icebreaker Oden and the Swedish Polar Research Secretariat (SPRS). BAL is supported by funding from the Research Council of Norway projects: CAATEX [280531] and HAVOC [280292]. We thank Mario Hoppmann, Philipp Anhaus and Matthieu Labaste for their help in conducting the ROV observations. The modeled light fields are available at https://doi.org/10.5281/zenodo.4491700 [*Katlein and Langelier*, 2021].

Author contribution statement

CK and SLG developed the concept for this study. QH provided the ridge geometry, JPL, AO and FLD ran the ray tracing simulations with Zemax. BAL, MB, ST provided guidance, interpretation and discussion of data and results. CK wrote and all authors contributed to editing of the manuscript.

References

Ackley, S. (1986), Sea-ice pressure ridge microbial, *Antarctic Journal of the United States*, *21*(5), 172.

Assmy, P., et al. (2013), Floating Ice-Algal Aggregates below Melting Arctic Sea Ice, *PLoS ONE*, *8*(10), e76599, doi:10.1371/journal.pone.0076599.

Bouguer, P. (1729), *Essai d'Optique*, Claude Jombert.

Castellani, G., R. Gerdes, M. Losch, and C. Lüpkes (2015), Impact of Sea-Ice Bottom Topography on the Ekman Pumping, in *Towards an Interdisciplinary Approach in Earth System Science: Advances of a Helmholtz Graduate Research School*, edited by G. Lohmann, H. Meggers, V. Unnithan, D. Wolf-Gladrow, J. Notholt and A. Bracher, pp. 139-148, Springer International Publishing, Cham, doi:10.1007/978-3-319-13865-7_16.

Castellani, G., C. Lüpkes, S. Hendricks, and R. Gerdes (2014), Variability of Arctic sea-ice topography and its impact on the atmospheric surface drag, *Journal of Geophysical Research: Oceans*, *119*(10), 6743-6762, doi:https://doi.org/10.1002/2013JC009712.

Davis, N. R., and P. Wadhams (1995), A statistical analysis of Arctic pressure ridge morphology, *Journal of Geophysical Research: Oceans*, *100*(C6), 10915-10925, doi:10.1029/95jc00007.

Fernández-Méndez, M., et al. (2018), Algal Hot Spots in a Changing Arctic Ocean: Sea-Ice Ridges and the Snow-Ice Interface, *Frontiers in Marine Science*, *5*(75), doi:10.3389/fmars.2018.00075.

359 Furgal, C. M., K. M. Kovacs, and S. Innes (1996), Characteristics of ringed seal, Phoca hispida,
360 subnivean structures and breeding habitat and their effects on predation, *Canadian Journal of*
361 *Zoology*, *74*(5), 858-874, doi:10.1139/z96-100.

362 Gradinger, R., B. Bluhm, and K. Iken (2010), Arctic sea-ice ridges-Safe heavens for sea-ice
363 fauna during periods of extreme ice melt?, *Deep-Sea Research Part Ii-Topical Studies in*
364 *Oceanography*, *57*(1-2), 86-95, doi:10.1016/j.dsr2.2009.08.008.

365 Haas, C., A. Pfaffling, S. Hendricks, L. Rabenstein, J.-L. Etienne, and I. Rigor (2008), Reduced
366 ice thickness in Arctic Transpolar Drift favors rapid ice retreat, *Geophys. Res. Lett.*, *35*(17),
367 L17501, doi:10.1029/2008gl034457.

368 Hisette, Q., A. Alekseev, and J. Seidel (2017), Discrete Element Simulation of Ship Breaking
369 Through Ice Ridges, in *The 27th International Ocean and Polar Engineering Conference*, edited,
370 p. 9, International Society of Offshore and Polar Engineers, San Francisco, California, USA.

371 Hop, H., M. Poltermann, O. J. Lønne, S. Falk-Petersen, R. Korsnes, and W. P. Budgell (2000),
372 Ice amphipod distribution relative to ice density and under-ice topography in the northern
373 Barents Sea, *Polar Biol.*, *23*(5), 357-367, doi:10.1007/s003000050456.

374 Horner, R., S. F. Ackley, G. S. Dieckmann, B. Gulliksen, T. Hoshiai, L. Legendre, I. A.
375 Melnikov, W. S. Reeburgh, M. Spindler, and C. W. Sullivan (1992), Ecology of Sea Ice Biota .1.
376 Habitat, Terminology, and Methodology, *Polar Biol.*, *12*(3-4), 417-427.

377 Høyland, K. V. (2002), Consolidation of first-year sea ice ridges, *Journal of Geophysical*
378 *Research: Oceans*, *107*(C6), 15-11-15-16, doi:10.1029/2000jc000526.

379 Hunkeler, P. A., M. Hoppmann, S. Hendricks, T. Kalscheuer, and R. Gerdes (2016), A glimpse
380 beneath Antarctic sea ice: Platelet layer volume from multifrequency electromagnetic induction
381 sounding, *Geophys. Res. Lett.*, *43*(1), 222-231, doi:10.1002/2015gl065074.

382 Katlein, C., S. Arndt, H. J. Belter, G. Castellani, and M. Nicolaus (2019), Seasonal Evolution of
383 Light Transmission Distributions Through Arctic Sea Ice, *Journal of Geophysical Research:*
384 *Oceans*, *124*, doi:https://doi.org/10.1029/2018JC014833.

385 Katlein, C., et al. (2015), Influence of ice thickness and surface properties on light transmission
386 through Arctic sea ice, *Journal of Geophysical Research: Oceans*, *120*(9), 5932-5944,
387 doi:10.1002/2015JC010914.

388 Katlein, C., M. Fernández-Méndez, F. Wenzhöfer, and M. Nicolaus (2014), Distribution of algal
389 aggregates under summer sea ice in the Central Arctic, *Polar Biol.*, 1-13, doi:10.1007/s00300-
390 014-1634-3.

391 Katlein, C., and J.-P. Langelier (2021), Computed Light Fields Within a Sea Ice Pressure Ridge,
392 edited, Zenodo, doi:10.5281/zenodo.4491701.

393 Katlein, C., D. K. Perovich, and M. Nicolaus (2016), Geometric Effects of an Inhomogeneous
394 Sea Ice Cover on the under Ice Light Field, *Frontiers in Earth Science*,
395 doi:10.3389/feart.2016.00006.

396 Katlein, C., L. Valcic, S. Lambert-Girard, and M. Hoppmann (2021), New insights into radiative
397 transfer within sea ice derived from autonomous optical propagation measurements, *The*
398 *Cryosphere*, *15*(1), 183-198, doi:10.5194/tc-15-183-2021.

399 Kwok, R., and D. A. Rothrock (2009), Decline in Arctic sea ice thickness from submarine and
400 ICESat records: 1958-2008, *Geophys. Res. Lett.*, *36*, doi:10.1029/2009gl039035.

401 Lambert, J. H. (1760), *Photometria*.

402 Lange, B. A., et al. (2017a), Pan-Arctic sea ice-algal chl a biomass and suitable habitat are
403 largely underestimated for multiyear ice, *Global Change Biology*, *23*(11), 4581-4597,
404 doi:10.1111/gcb.13742.

405 Lange, B. A., et al. (2019), Contrasting Ice Algae and Snow-Dependent Irradiance Relationships
406 Between First-Year and Multiyear Sea Ice, *Geophys. Res. Lett.*, *46*(19), 10834-10843,
407 doi:10.1029/2019gl082873.

408 Lange, B. A., C. Katlein, G. Castellani, M. Fernández-Méndez, M. Nicolaus, I. Peeken, and H.
409 Flores (2017b), Characterizing Spatial Variability of Ice Algal Chlorophyll a and Net Primary
410 Production between Sea Ice Habitats Using Horizontal Profiling Platforms, *Frontiers in Marine*
411 *Science*, *4*(349), doi:10.3389/fmars.2017.00349.

412 Leppäranta, M., and R. Hakala (1992), The structure and strength of first-year ice ridges in the
413 Baltic Sea, *Cold Reg. Sci. Tech.*, *20*(3), 295-311, doi:https://doi.org/10.1016/0165-
414 232X(92)90036-T.

415 Light, B., T. C. Grenfell, and D. K. Perovich (2008), Transmission and absorption of solar
416 radiation by Arctic sea ice during the melt season, *J. Geophys. Res.-Oceans*, *113*(C3),
417 doi:10.1029/2006jc003977.

418 Light, B., D. K. Perovich, M. A. Webster, C. Polashenski, and R. Dadic (2015), Optical
419 properties of melting first-year Arctic sea ice, *Journal of Geophysical Research: Oceans*,
420 *120*(11), 7657-7675, doi:10.1002/2015JC011163.

421 Maslanik, J. A., C. Fowler, J. Stroeve, S. Drobot, J. Zwally, D. Yi, and W. Emery (2007), A
422 younger, thinner Arctic ice cover: Increased potential for rapid, extensive sea-ice loss, *Geophys.*
423 *Res. Lett.*, *34*(24), L24501, doi:10.1029/2007gl032043.

424 Maslanik, J. A., J. Stroeve, C. Fowler, and W. Emery (2011), Distribution and trends in Arctic
425 sea ice age through spring 2011, *Geophys. Res. Lett.*, *38*, doi:10.1029/2011gl047735.

426 Massicotte, P., I. Peeken, C. Katlein, H. Flores, Y. Huot, G. Castellani, S. Arndt, B. A. Lange, J.
427 É. Tremblay, and M. Babin (2019), Sensitivity of phytoplankton primary production estimates to

428 available irradiance under heterogeneous sea ice conditions, *Journal of Geophysical Research:*
429 *Oceans*, *124*(8), 5436-5450.

430 Matthes, L. C., J. K. Ehn, S. L.-Girard, N. M. Pogorzelec, M. Babin, and C. J. Mundy (2019),
431 Average cosine coefficient and spectral distribution of the light field under sea ice: Implications
432 for primary production., *Elem Sci Anth*, *7*(1), doi:http://doi.org/10.1525/elementa.363.

433 Meier, W. N., et al. (2014), Arctic sea ice in transformation: A review of recent observed
434 changes and impacts on biology and human activity, *Rev Geophys*, *52*(3), 185-217, doi:Doi
435 10.1002/2013rg000431.

436 Melling, H., D. R. Topham, and D. Riedel (1993), Topography of the upper and lower surfaces
437 of 10 hectares of deformed sea ice, *Cold Reg. Sci. Tech.*, *21*(4), 349-369,
438 doi:https://doi.org/10.1016/0165-232X(93)90012-W.

439 Melnikov, I. A. (1997), The Arctic sea ice ecosystem, edited, Cambridge Univ Press.

440 Melnikov, I. A., and L. L. Bondarchuk (1987), To the ecology of the mass aggregations of
441 colonial diatom algae under the Arctic drifting sea ice, *Okeanologiya*, *27*(2), 317-321.

442 Mobley, C. D. (1994), *Light and water: radiative transfer in natural waters*, Academic Press.

443 Mobley, C. D., G. F. Cota, T. C. Grenfell, R. A. Maffione, W. S. Pegau, and D. K. Perovich
444 (1998), Modeling light propagation in sea ice, *IEEE Transactions on Geoscience and Remote*
445 *Sensing 36*(5), 1743-1749, doi:10.1109/36.718642.

446 Nicolaus, M., C. Katlein, J. Maslanik, and S. Hendricks (2012), Changes in Arctic sea ice result
447 in increasing light transmittance and absorption, *Geophys. Res. Lett.*, *39*, L24501,
448 doi:10.1029/2012gl053738.

449 Nuber, A., L. Rabenstein, J. A. Lehmann-Horn, M. Hertrich, S. Hendricks, A. Mahoney, and H.
450 Eicken (2017), Water content estimates of a first-year sea-ice pressure ridge keel from surface-
451 nuclear magnetic resonance tomography, *Ann. Glaciol.*, *54*(64), 33-43,
452 doi:10.3189/2013AoG64A205.

453 Perovich, D. K. (1990), Theoretical estimates of light reflection and transmission by spatially
454 complex and temporally varying sea ice covers, *J. Geophys. Res.-Oceans*, *95*(C6), 9557-9567,
455 doi:10.1029/JC095iC06p09557.

456 Pilfold, N. W., A. E. Derocher, I. Stirling, and E. Richardson (2014), Polar bear predatory
457 behaviour reveals seascape distribution of ringed seal lairs, *Population Ecology*, *56*(1), 129-138,
458 doi:10.1007/s10144-013-0396-z.

459 Rabenstein, L., A. Nuber, J. A. Lehmann-Horn, M. Hertrich, S. Hendricks, A. R. Mahoney, and
460 H. Eicken (2013), Porosity of a sea-ice pressure ridge keel estimated on the basis of surface
461 nuclear magnetic resonance measurements.

462 Rampal, P., J. Weiss, and D. Marsan (2009), Positive trend in the mean speed and deformation
463 rate of Arctic sea ice, 1979–2007, *Journal of Geophysical Research: Oceans*, *114*(C5), C05013,
464 doi:10.1029/2008JC005066.

465 Richter-Menge, J. A., and G. F. N. Cox (1985), Structure, Salinity and Density of Multi-Year
466 Sea Ice Pressure Ridges, *Journal of Energy Resources Technology*, *107*(4), 493-497,
467 doi:10.1115/1.3231224.

468 Siegel, V., B. Bergström, J. O. Strömberg, and P. H. Schalk (1990), Distribution, size
469 frequencies and maturity stages of krill, Euphausia superba, in relation to sea-ice in the Northern
470 Weddell Sea, *Polar Biol.*, *10*(7), 549-557, doi:10.1007/BF00233705.

471 Smith, T. G., M. O. Hammill, and G. TaugbØl (1991), A Review of the Developmental,
472 Behavioural and Physiological Adaptations of the Ringed Seal, Phoca Hispida, to Life in the
473 Arctic Winter, *Arctic*, *44*(2), 124-131.

474 Strub-Klein, L., and D. Sudom (2012), A comprehensive analysis of the morphology of first-year
475 sea ice ridges, *Cold Reg. Sci. Tech.*, *82*, 94-109,
476 doi:https://doi.org/10.1016/j.coldregions.2012.05.014.

477 Sturm, M., J. Holmgren, and D. K. Perovich (2002), Winter snow cover on the sea ice of the
478 Arctic Ocean at the Surface Heat Budget of the Arctic Ocean (SHEBA): Temporal evolution and
479 spatial variability, *Journal of Geophysical Research: Oceans*, *107*(C10), SHE 23-21-SHE 23-17,
480 doi:https://doi.org/10.1029/2000JC000400.

481 Timco, G. W., and R. P. Burden (1997), An analysis of the shapes of sea ice ridges, *Cold Reg.*
482 *Sci. Tech.*, *25*(1), 65-77, doi:https://doi.org/10.1016/S0165-232X(96)00017-1.

483 Wadhams, P., and N. Toberg (2012), Changing characteristics of arctic pressure ridges, *Polar*
484 *Science*, *6*(1), 71-77, doi:https://doi.org/10.1016/j.polar.2012.03.002.

485 Warren, S. G., and R. E. Brandt (2008), Optical constants of ice from the ultraviolet to the
486 microwave: A revised compilation, *Journal of Geophysical Research: Atmospheres*, *113*(D14),
487 doi:https://doi.org/10.1029/2007JD009744.

488 Williams, G. D., et al. (2013), Beyond Point Measurements: Sea Ice Floes Characterized in 3-D,
489 *Eos, Transactions American Geophysical Union*, *94*(7), 69-70, doi:10.1002/2013EO070002.

490 Williams, G. D., T. Maksym, J. Wilkinson, C. Kunz, C. Murphy, P. Kimball, and H. Singh
491 (2015), Thick and deformed Antarctic sea ice mapped with autonomous underwater vehicles,
492 *Nature Geosci*, *8*(1), 61-67, doi:10.1038/ngeo2299.
493